Brazilian Journal of Physics (2019) 49:628–635
https://doi.org/10.1007/s13538-019-00692-3

SOCIEDADE BRASILEIRA DE FÍSICA

CONDENSED MATTER

LO-Phonon-Limited Electron Mobility in a Core-Shell Polar Semiconductor Quantum Wire

Nguyen Nhu Dat[1,2] · **Le Thanh Hai**[3]

Received: 14 May 2019 / Published online: 16 July 2019

Abstract

Electron scattering rate and electron mobility limited by LO-phonons are calculated for a cylindrical polar semiconductor quantum wire with core-shell structure. Longitudinal optical phonons modes are developed within a dielectric continuum model. The influence of the thickness of the shell on the electron scattering rate by phonons is studied. Numerical calculations performed for a GaAs/AlGaAs quantum wire show that the electron–LO-phonon scattering rate changes with the thickness of the shell layer and is reduced considerably in the quantum wires having thicker shell, leading to higher electron mobility. The mobility can be improved up to several orders of magnitude.

Keywords Core-shell quantum wire · LO-phonon · Electron mobility · Shell thickness

1 Introduction

Nowadays the nanoscale semiconductor structures such as quantum wires are available thanks to the developments in semiconductor technology and have potential applications in high-speed devices [1–6]. Due to the reduction in impurity scattering in these quasi-one-dimensional systems, phonon scattering determines electron mobility at room temperature and the dynamics of electron-phonon systems. In these structures, the electron scattering rate is affected not only by the confinement of electrons but also by the changes in the phonon modes [7, 8]. These changes, therefore, strongly affect the transport properties of electrons in quantum wires.

In existing literature, optical phonons and their interaction with electrons have been developed mostly for free-standing quantum wires [9–11] or for quantum wires embedded in another infinite material [12–14]. Recently, many theoretical and experimental studies have been devoted to core-shell quantum wires, showing a lot of their properties related to the existence of the shell layer. The authors of Ref. [15] showed theoretically the thermal conductivity in core-shell Si/Ge nanowires can be drastically reduced by relevant combinations of the wire cross-section modulation and the mismatch between the core and shell acoustic impedances. The thermal conductivity in core-shell nanowires can also be reduced by structural defects non-uniformly distributed in the shell [16]. Magnetoconductance measurements at low temperature performed on GaAs/InAs core-shell nanowires [17–19] revealed Aharonov-Bohm type oscillations attributed to electron transport within the shell through angular momentum states. The temperature dependence of electron mobility measured on core-shell InAs/InAlAs nanowires [20] is an evidence for an effect of the shell in reducing surface states leading to reduction in ionized impurity scattering. Santiago-Pérez D. G. et al. [21] have considered Ge/Si and Si/Ge core-shell nanowires, studied and discussed the role of the shell on the acoustical phonons and their interaction with electrons via deformation potential mechanism.

In this work, we study the effect of the thickness of the shell layer on electron scattering and mobility limited by LO-phonons in a quantum wire with core-shell structure. In Section 2, we write down the expression for the relative atomic displacement corresponding to optical longitudinal

✉ Nguyen Nhu Dat
nguyennhudat@dtu.edu.vn; nndat@iop.vast.ac.vn

1 Institute of Theoretical and Applied Research, Duy Tan University, 73 Hoang Cau, Hanoi 100000, Vietnam

2 Institute of Physics, Vietnam Academy of Science and Technology, 10 Dao Tan, Hanoi 100000, Vietnam

3 Hanoi University of Civil Engineering, 55 Giai phong, Hanoi 100000, Vietnam

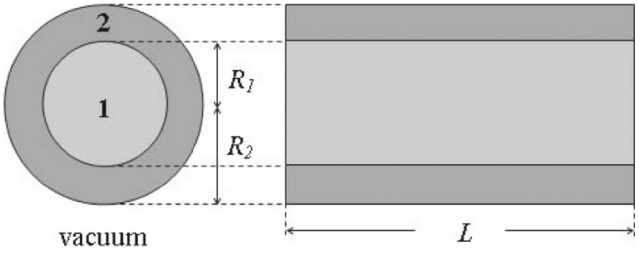

Fig. 1 Geometry of the circular wire: 1 and 2 are the core and shell materials, respectively

vibrations and give the classification of possible phonon modes in a core-shell quantum wire. We show also the change of phonon frequencies with the shell thickness. Section 3 is devoted to calculations of phonon scattering and electron mobility for core-shell quantum wires with various thickness of the shell layer. Our results are summarized in Section 4.

2 LO-Phonon modes

Let us consider a model of a semiconductor quantum wire of length L (assumed large) with circular cross-section (Fig. 1). The wire has a core of the shape of a cylinder with radius R_1 made of a polar material (1). The core is surrounded by a coaxial cylindrical layer of another polar material (2) of thickness $d = R_2 - R_1$. The infinite space around the wire is assumed to be vacuum. We use the polar coordinates r, φ, and z with the wire axis being chosen as the z axis. For practical dimension of quantum wires we may employ the dielectric continuum model to develop LO-phonon modes. The details can be found in our previous paper [22] and some main points are outlined below for completeness, using the same notations as in it.

The relative atomic displacement corresponding to the eigenfields of LO-phonons can be written as

$$u_{\nu mq}(x) = \nabla \left\{ \psi_{\nu mq}(r) \frac{1}{\sqrt{2\pi L}} e^{\mathrm{i}(m\varphi+qz)} \right\} \tag{1}$$

and has the explicit form

$$u_{\nu mq}(x) = \frac{1}{\sqrt{2\pi L}} e^{\mathrm{i}(m\varphi+qz)} u_{\nu mq}(r)$$
$$= \frac{1}{\sqrt{2\pi L}} e^{\mathrm{i}(m\varphi+qz)}$$
$$\times \begin{cases} A\left[q_1 F'_m(q_1 r) e_r + \mathrm{i}\frac{m}{r} F_m(q_1 r) e_\varphi + \mathrm{i}q F_m(q_1 r) e_z\right] \\ \qquad\qquad \text{for } r < R_1 , \\ q_2\left[B\, F'_m(q_2 r) + C\, G'_m(q_2 r)\right] e_r \\ \quad + \mathrm{i}\frac{m}{r}\left[B\, F_m(q_2 r) + C\, G_m(q_2 r)\right] e_\varphi \\ \quad + \mathrm{i}q\left[B\, F_m(q_2 r) + C\, G_m(q_2 r)\right] e_z \\ \qquad\qquad \text{for } R_1 \le r \le R_2 . \end{cases} \tag{2}$$

The phonon frequency ω is indexed by the set νmq ($\omega \equiv \omega_{\nu mq}$) and determined by the following dispersion equation

$$\begin{aligned} &\varepsilon_{1\infty} q_1 F'_m(q_1 R_1) \\ &\quad \times \left\{ q K'_m(q R_2) \left[F_m(q_2 R_1) G_m(q_2 R_2) \right.\right. \\ &\qquad \left. - G_m(q_2 R_1) F_m(q_2 R_2)\right] \\ &\qquad + \varepsilon_{2\infty} q_2 K_m(q R_2) \left[G_m(q_2 R_1) F'_m(q_2 R_2) \right. \\ &\qquad \left.\left. - F_m(q_2 R_1) G'_m(q_2 R_2)\right]\right\} \\ &+ \varepsilon_{2\infty} q_2 F_m(q_1 R_1) \\ &\quad \times \left\{ q K'_m(q R_2) \left[G'_m(q_2 R_1) F_m(q_2 R_2) \right.\right. \\ &\qquad \left. - F'_m(q_2 R_1) G_m(q_2 R_2)\right] \\ &\qquad + \varepsilon_{2\infty} q_2 K_m(q R_2) \left[F'_m(q_2 R_1) G'_m(q_2 R_2) \right. \\ &\qquad \left.\left. - G'_m(q_2 R_1) F'_m(q_2 R_2)\right]\right\} \\ &\qquad = 0 . \end{aligned} \tag{3}$$

The notation $\nu \equiv (tn)$ consists of two indexes: t indicating the type of the phonon mode and the integer n labeling the roots of (3) which are ordered decreasing gradually (in [22] the roots are labeled in the opposite order). Depending on whether the quantities q_1 and q_2 are real or imaginary we have different phonon types. The indexes (mn) denote different phonon branches of type t. Table 1 gives the classification of the longitudinal optical phonon modes in a core-shell quantum wire.

Table 1 LO-phonon modes of core-shell cylindrical quantum wires

Type of modes t	q_j	$\psi_{\nu mq}(r)$	
		$r < R_1$	$R_1 < r < R_2$
1	real q_1, real q_2	$A\ \mathrm{J}_m(q_1 r)$	$B\,\mathrm{J}_m(q_2 r) + C\,\mathrm{Y}_m(q_2 r)$
2	real q_1, imaginary q_2	$A\,\mathrm{J}_m(q_1 r)$	$B\,\mathrm{I}_m(\xi_2 r) + C\,\mathrm{K}_m(\xi_2 r)$
3	imaginary q_1, real q_2	$A\,\mathrm{I}_m(\xi_1 r)$	$B\,\mathrm{J}_m(q_2 r) + C\,\mathrm{Y}_m(q_2 r)$
4	imaginary q_1, imaginary q_2	$A\,\mathrm{I}_m(\xi_1 r)$	$B\,\mathrm{I}_m(\xi_2 r) + C\,\mathrm{K}_m(\xi_2 r)$

For illustration, we consider a GaAs/$Al_{0.3}Ga_{0.7}As$ quantum wire. The parameters for $Al_xGa_{1-x}As$ are taken from Ref. [23], namely:

$$\begin{aligned}\varepsilon_\infty &= 10.89 - 2.73x\\ \varepsilon_0 &= 12.90 - 2.84\,x\\ \omega_L &= 36.25 + 1.83x + 17.12x^2 - 5.11x^3\ (\text{meV})\\ v_L &= (4.73 + 0.68x + 0.24x^2)\ (10^5\text{cm/s})\end{aligned}$$

The existence of phonons of a type depends on the concrete material parameters. Numerical calculations show that there exist only phonons of type 1 and type 3 in quantum wires under consideration. In Fig. 2, we plot the wave-vector dispersions of the highest branch ($m = 0$, $n = 1$) for phonons in quantum wires of the same radius R_1 but with various thickness d of the shell. As seen from the figures, the change in the shell thickness does not affect the q-dependence of the phonon frequencies for both phonon types. The dependence of frequencies on the shell thickness, however, is quite different for these two types of phonons as depicted in Fig. 3. The frequency of type 1 phonons does not vary continuously with the shell thickness but changes abruptly at certain thicknesses which are nearly equispaced. Meanwhile, the frequency of type 3 phonons initially increases with increasing thickness and then, beyond the thickness of about 5 nm, it changes very little for all values of the core radius.

3 LO-Phonon Scattering and Electron Mobility

We can express the electrostatic potential $\phi(x)$ related to the displacement $u_{vmq}(x)$ as

$$\phi_{vmq}(x) = \eta_{vmq}(r)\,\frac{1}{\sqrt{2\pi L}}\,e^{i(m\varphi+qz)} \tag{4}$$

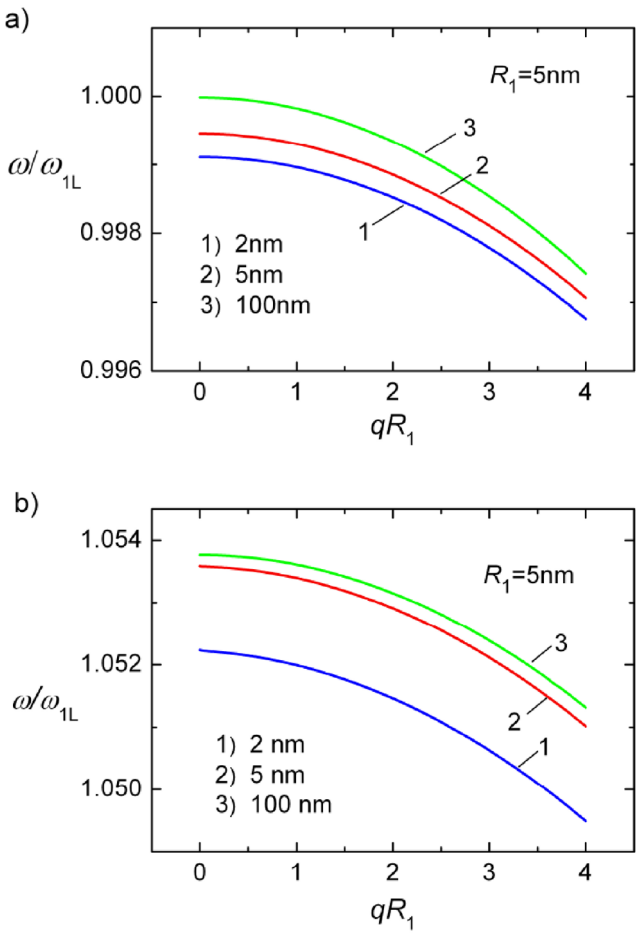

Fig. 2 Dispersion curves of phonons of the uppermost branch with $(m = 0, n = 1)$ in a GaAs/$Al_{0.3}Ga_{0.7}As$ quantum wire with $R_1 = 5$ nm and with various thickness of the shell (1) $d = 2$ nm, (2) 5 nm, and (3) 100 nm: **a** type 1 phonons, **b** type 3 phonons

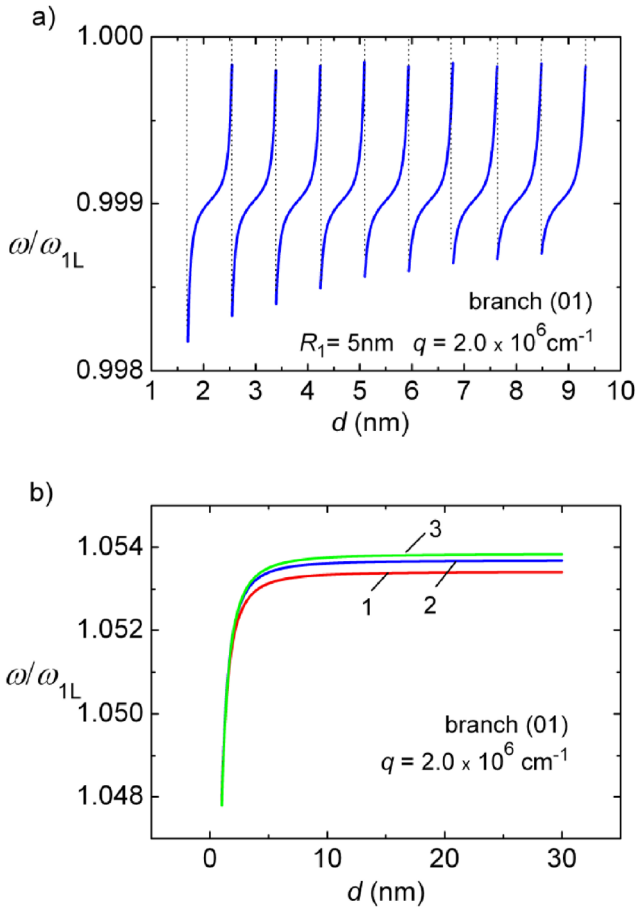

Fig. 3 The dependence of phonon frequency on the shell thickness for phonons of the uppermost branch $(m = 0, n = 1)$ at $q = 2.0 \times 10^6\,\text{cm}^{-1}$ in a GaAs/$Al_{0.3}Ga_{0.7}As$ quantum wire with various values of the core radius: **a** phonons of type 1, $R_1 = 5$ nm; **b** phonons of type 3, $R_1 = 3$ nm (1), 5 nm (2), and 50 nm (3)

with the radial part given by

$$\eta_{vmq}(r) = 4\pi \left[N_1 e_1^* \,\Theta(R_1 - r) + N_2 e_2^* \,\Theta(R_2 - r)\,\Theta(r - R_1)\right] \psi_{vmq}(r)\,, \tag{5}$$

where $\Theta(x)$ is the Heaviside step function.

The radial part of the electrostatic potentials associated with LO-modes is plotted in Fig. 4 in relative units for two highest branches, i.e., the potentials are compared with the maximum value of the potential associated with phonon mode (01). This maximum value is of order of 10^{-5} V for oscillations of 10^{-3} nm in a wire with core radius $R_1 = 5$ nm and shell thickness $d = 5$ nm. It is seen that the potential is more pronounced in the core region for phonon modes of type 1 and, on the contrary, in the shell for type 3 phonon modes. Furthermore, the potential associated with phonons of type 1 oscillates in the shell region more rapidly for wires with thicker shell, leading to smaller interaction energy of electrons moving in the shell. It would be expected that the electron being in the core region would interact mainly with phonons of type 1 and the electron in the shell mainly with phonons of type 3.

The scattering rates are normally calculated via Fermi's golden rule with the Hamiltonian

$$H = -\frac{e}{2}\left(\phi(x) + \phi^*(x)\right)\,. \tag{6}$$

For an electron in state Ψ_α, the scattering rate by optical phonons is given by

$$\Gamma = \frac{2\pi}{\hbar} \sum_{\Psi_{\alpha'}} \sum_{\xi} \sum_{\zeta=\pm 1} \left|B_{\alpha'\alpha\xi}\right|^2 \left(n(\omega_\xi) + \frac{1}{2} + \zeta\frac{1}{2}\right) \times (1 - N_{\alpha'})\;\delta(E_{\alpha'} - E_\alpha + \zeta\hbar\omega_\xi)\,. \tag{7}$$

Here α (α') represents the set of quantum numbers determining the electron state Ψ_α ($\Psi_{\alpha'}$). The notation $\xi \equiv (vmq)$ denotes phonon modes. The electron-phonon interaction matrix element $B_{\alpha'\alpha\xi}$ is given by

$$B_{\alpha'\alpha\xi} = \langle \Psi_{\alpha'} \mid e\eta_\xi(r)\mathrm{e}^{i(m\varphi+qz)} \mid \Psi_\alpha \rangle\,.$$

N_α is the electron distribution function, $n(\omega_\xi)$ is the phonon occupation factor, and E_α is the electron energy. In (7), $\zeta = +1\,(-1)$ corresponds to emission (absorption) of a phonon.

For simplicity, electrons are assumed to be confined in the infinitely deep potential well

$$V(x) = \begin{cases} 0 & \text{for } r \le R_1\,, \\ V_0 > 0 & \text{for } R_1 < r \le R_2\,, \\ \infty & \text{for } R_2 < r\,. \end{cases} \tag{8}$$

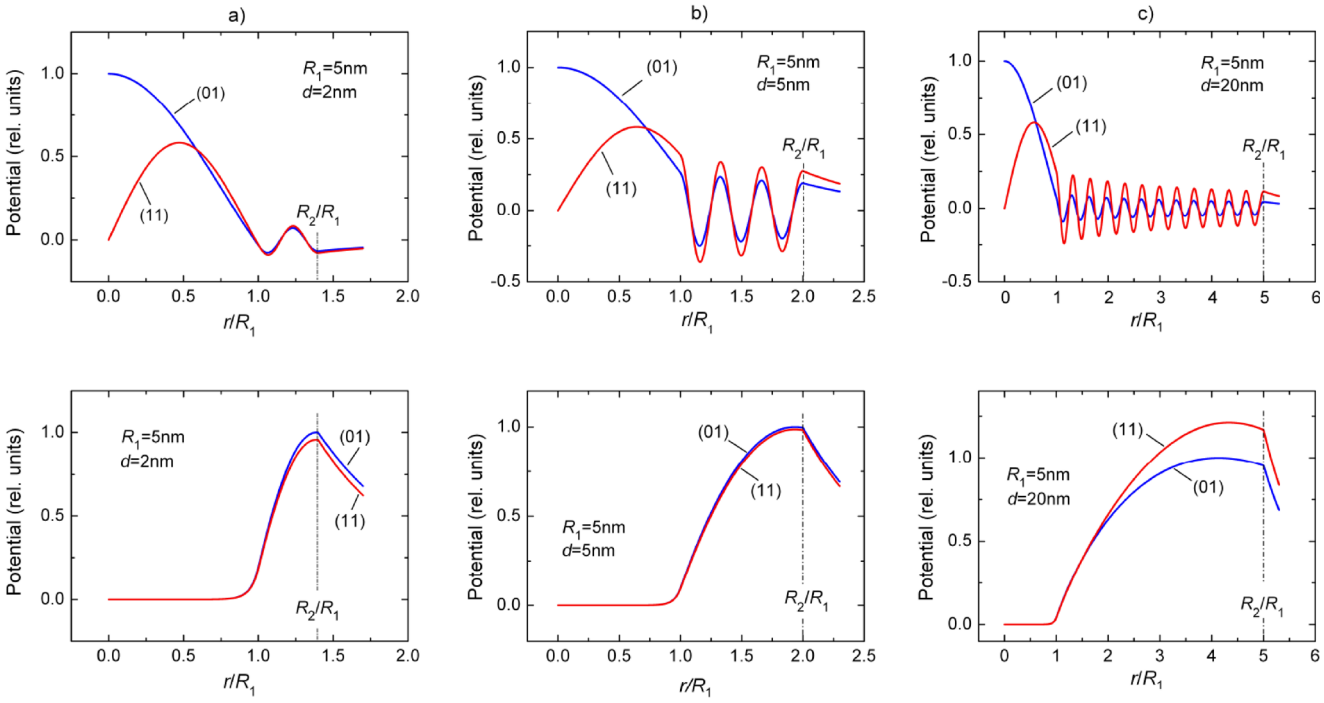

Fig. 4 Electrostatic potentials related to phonon modes (mn) of type 1 (upper row) and type 3 (lower row) for a GaAs/$Al_{0.3}Ga_{0.7}As$ quantum wire with core radius $R_1 = 5$ nm and various thickness of the shell d: **a** 2 nm, **b** 5 nm, and **c** 20 nm. The wave number q is taken so as $qR_1 = 1$

Within the effective mass approximation, the electron envelope wave function can be written in the form

$$\Psi_\alpha \equiv \Psi_{lnk}(x) = \frac{1}{\sqrt{2\pi L}} e^{i(l\varphi+kz)} \times \begin{cases} A\, F_l(\upsilon r) & \text{for } r < R_1\,, \\ B\, F_l(\kappa r) + C\, G_l(\kappa r) & \text{for } R_1 \le r \le R_2\,, \\ 0 & \text{for } R_2 < r\,. \end{cases} \quad (9)$$

Here, the constants A, B, and C are defined by the normalization of the eigenfunctions. The possible values of the electron wave vector are $k = (2\pi m)/L$ with integer m. The energy $E_\alpha \equiv E_{ln}(k)$ associated with the state Ψ_{lnk} is specified by quantum numbers l and n as subband indexes and defined by a root of the equation

$$\begin{aligned} & m_2 \upsilon F_l'(\upsilon R_1)\,[F_l(\kappa R_1)G_l(\kappa R_2) - F_l(\kappa R_2)G_l(\kappa R_1)] \\ & + m_1 \kappa F_l(\upsilon R_1)\left[F_l(\kappa R_2)G_l'(\kappa R_1) - F_l'(\kappa R_1)G_l(\kappa R_2)\right] \\ & = 0 \end{aligned} \quad (10)$$

with n corresponding to the nth root of the equation. Here we use the notation

$$\upsilon = \sqrt{\frac{2m_1}{\hbar^2}E - k^2}\,,$$
$$\kappa = \sqrt{\frac{2m_2}{\hbar^2}(E - V_0) - k^2}$$

with m_1 and m_2 being the electron effective mass in material 1 and material 2, respectively. In analogy with the case of phonons in Section 2, the functions F_l and G_l are Bessel functions J_l and Y_l or modified Bessel functions I_l and K_l of order l [24], respectively, depending on whether the quantities υ and κ are real or imaginary.

Figure 5 illustrates the dispersion of the two lowest electron energy subbands. It should be noted that if one assumes the same electron effective mass m_{eff} in both core and shell materials, the subband dispersion is parabolic

$$E_{par} = E_{ln}(0) + \frac{\hbar^2 k^2}{2m_{eff}}\,. \quad (11)$$

The k-dependence of the subband energy, in fact, differs from the parabolic law as depicted in Fig. 6. It is evident that the subband non-parabolicity is stronger in the wire with thicker shell (Fig. 6a) and for higher subbands (Fig. 6b). The deviation from parabolic law can reach several percent of V_0 at reasonable values of k. As seen in Fig. 6b, the deviation is 0.4% and 3% for subband (01) and 1.2% and 8% for subband (11) at the wave vector k with $kR_1 = 1.25$ and $kR_1 = 3$, respectively, in the wire with the shell thickness

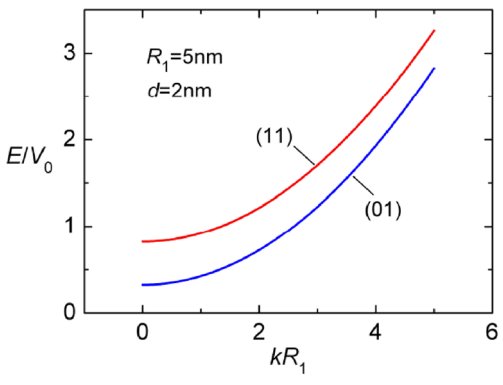

Fig. 5 Electron energy dispersion of the two lowest subbands (01) and (11) for a GaAs/$Al_{0.3}Ga_{0.7}$As quantum wire with radius $R_1 = 5$ nm and shell thickness $d = 2$ nm. Conduction band discontinuity at GaAs/$Al_{0.3}Ga_{0.7}$As heterointerface is $V_0 = 0.237$ eV

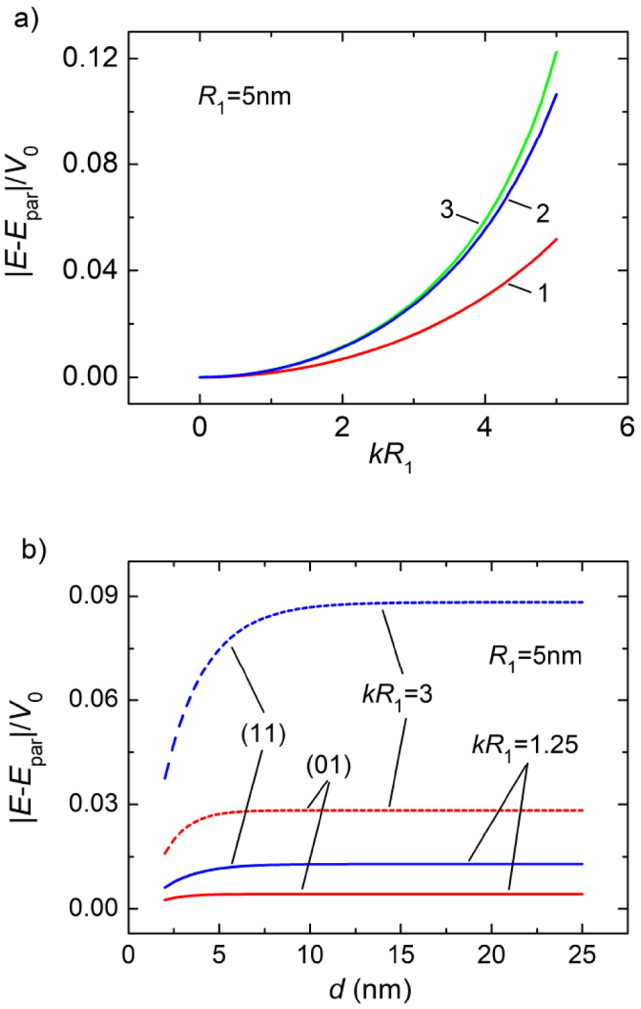

Fig. 6 Deviation of the actual electron subband energy from the parabolic one when assumed the electron mass in the shell and in the core is the same ($m_{eff} = m_1$): **a** as a function of electron wave vector k for subbands (01), the shell thickness is 2 nm (1), 5 nm (2), and 20 nm (3); **b** as a function of shell thickness for subbands (01) and (11) at electron wave vector k with $kR_1 = 1.25$ and $kR_1 = 3$. The numerical calculation is performed for a GaAs/$Al_{0.3}Ga_{0.7}$As quantum wire with the core radius $R_1 = 5$ nm

of 5 nm. The deviation increases as the shell thichness increases and almost does not change for larger thickness. It is worth to note this non-parabolicity is coming from the difference in electron effective masses of the constitutive materials, not from the energy band non-parabolicity of the materials.

As pointed out in [25–27], the non-parabolicity of the energy bands leads to large optical nonlinearity by conduction electrons in bulk semiconductors. It would, therefore, be expected this effect is a new origin of large optical nonlinearity in lower dimension systems such as quantum wires and is the subject of another study.

In Fig. 7, we plotted the electron scattering rate by phonons of type 1 and of type 3 separately. For convenience, we express the rates in terms of the characteristic rate $\Gamma_0 = 8.7 \times 10^{12}\,\mathrm{s}^{-1}$ for bulk GaAs. It is seen that the former is nearly two orders of magnitude greater than the latter. This means type 1 phonons play a dominant role in interaction with electrons which, from what mentioned below Eq. (5), move in the core. On the other hand, in the wire of thicker shell, the electron wave function spreads into the shell region and, therefore, the probability for an electron being in the core is smaller. This reduces the electron-phonon interaction, leading to smaller scattering rate in wires with thicker shells.

Figure 8 illustrates the variation with the electron wave vector in the total electron scattering rates by LO-phonons for a quantum wire with radius of 5 nm at temperature of 300 K for various values of the shell thickness. It is seen that the rate in the wire with thinner shell is greater than the rate in the wire with thicker shell, as discussed above. The peaks in scattering rates at $kR_1 \approx 1.25$ (corresponding to electron energy of 0.232 eV and 0.213 eV for the wire with shell thickness of 2 nm and 5 nm, respectively) is due to resonant phonon emission. This is evident from Fig. 9 where

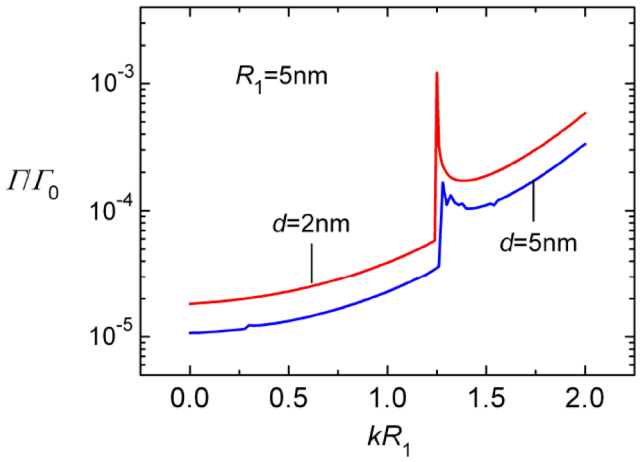

Fig. 8 Scattering rate by LO-phonons of an electron as a function of its wave vector k in a GaAs/$Al_{0.3}Ga_{0.7}$As wire at temperature $T = 300$ K for various values of the thickness d of the shell material. The radius of the core is 5 nm. The electron is in the subband $(l = 1, n = 1)$

scattering rates subject to phonon absorption or emission separately are plotted as a function of electron wave vector.

The electron mobility μ is usually given by

$$\mu = \frac{e}{m^*}\tau \tag{12}$$

where m^* is the effective mass of electron defined by the subband energy via the expression

$$\frac{1}{m^*} = \frac{1}{\hbar^2}\frac{\partial^2 E_{ln}(k)}{\partial k^2}\bigg|_{k=0}. \tag{13}$$

τ is the relaxation time which is a measure for electron momentum decay due to various kinds of scattering. We will adopt the memory function formalism [28] to calculate the relaxation time τ. Dropping the electron-electron interaction and restricting ourselves to the lowest order of electron-phonon interaction, we obtain the expression

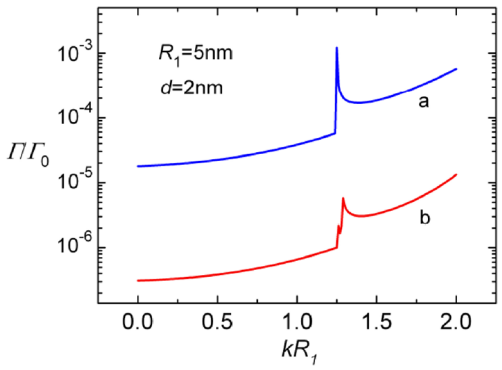

Fig. 7 Electron scattering rate by LO-phonons of type 1 (**a**) and type 3 (**b**) as a function of its wave vector k in a GaAs/$Al_{0.3}Ga_{0.7}$As wire. The radius of the core is 5 nm; the thickness of the shell is 2 nm. The electron is in the subband $(l = 1, n = 1)$

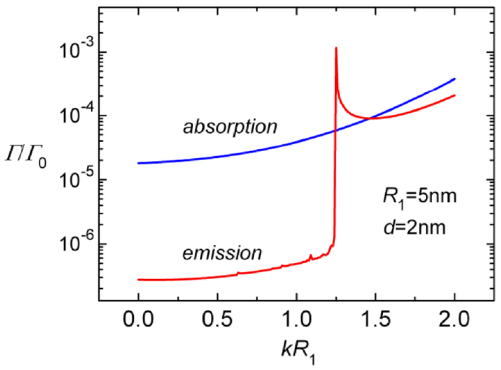

Fig. 9 LO-phonon absorption and emission rates as a function of electron wave vector k in a GaAs/$Al_{0.3}Ga_{0.7}$As wire with shell thickness of 2 nm at temperature $T = 300$ K. The radius of the core is 5 nm. The electron is in the subband $(l = 1, n = 1)$

for the electron relaxation time limited by LO-phonon scattering

$$\frac{1}{\tau} = \frac{2\pi m^*}{k_B T \hbar^3 n_e L} \sum_{\alpha\alpha'\xi} \left(\frac{\partial E_\alpha}{\partial k} - \frac{\partial E_{\alpha'}}{\partial k'} \right)^2 \mid B_{\alpha'\alpha\xi} \mid^2 \times N_\alpha \left(1 - N_{\alpha'}\right) n(\omega_\xi)\, \delta\left(E_{\alpha'} - E_\alpha - \hbar\omega_\xi\right) . \quad (14)$$

In the above equation, n_e is the electron linear density.

Figure 10 shows the temperature dependence of the total electron mobility and of the mobility subject to only intersubband or intrasubband scattering in core-shell GaAs/$Al_{0.3}Ga_{0.7}$As quantum wires. We have assumed the electrons occupy the subband ($l = 1, n = 1$). The linear electron density is taken as $1.0 \times 10^6\,\mathrm{cm}^{-1}$. The mobility decreases with increasing temperature. Moreover, it is seen that the intersubband scattering has the main contribution to the total mobility and, therefore, is the dominating mechanism in electron–LO-phonon interaction.

In Fig. 11 we plot the electron mobility as a function of temperature in core-shell GaAs/AlGaAs quantum wires with the same core dimension but different thickness of the shell.

It is shown that the electron mobility is higher in the wires with larger shell thickness in accordance with lower scattering rate mentioned above. Numerical calculation shows that electron mobility can be improved by two orders of magnitude in the wire with 5 nm radius when increasing the shell thickness from 2 to 5 nm.

The increase of electron mobility with increasing shell thickness in core-shell GaAs/AlGaAs nanowires was revealed experimentally and reported in Ref. [29]. The authors suggest that the improvement in carrier mobility can be attributed to the reduction of carrier scattering by charged surface states since thicker shells give greater separation of carriers from these scattering sites. In the present work, we suggest and explain another mechanism leading to higher electron mobility in quantum wires with thicker shell. The spreading of the electron wave function into the shell region leads to weaker interaction of electrons with phonons of type 1 and, therefore, to higher electron mobility.

The calculated mobility is rather higher than available experimental data in Ref. [29]. As shown in Fig. 12, the number of phonon branches increases rapidly when the size of the quantum wire increases. This opens up more

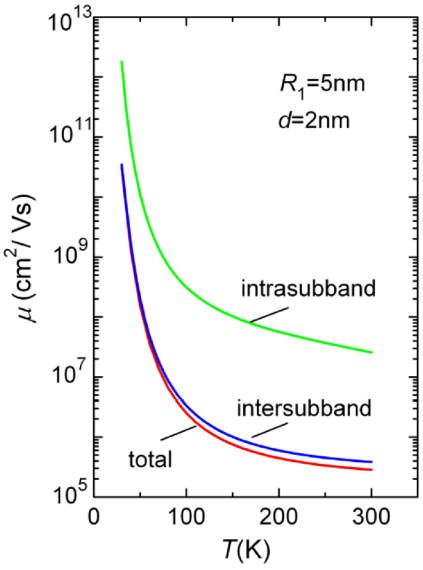

Fig. 10 The total electron mobility and the mobility subject to only intersubband or intrasubband scattering as a function of temperature in the GaAs/$Al_{0.3}Ga_{0.7}$As wire with the core radius 5 nm and the shell thickness of 2 nm. Electrons occupy subband ($l = 1, n = 1$) with the linear density of $1.0 \times 10^6\,\mathrm{cm}^{-1}$

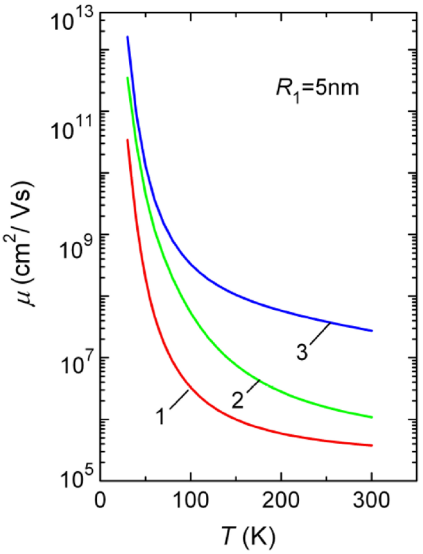

Fig. 11 Temperature dependence of phonon-limited electron mobility in a GaAs/$Al_{0.3}Ga_{0.7}$As wire. The radius of the core is 5 nm; the thickness of the shell is of 2 nm (1), 3 nm (2), and 5 nm (3). It is assumed the subband ($l = 1, n = 1$) is occupied by electrons with the linear density $1.0 \times 10^6\,\mathrm{cm}^{-1}$

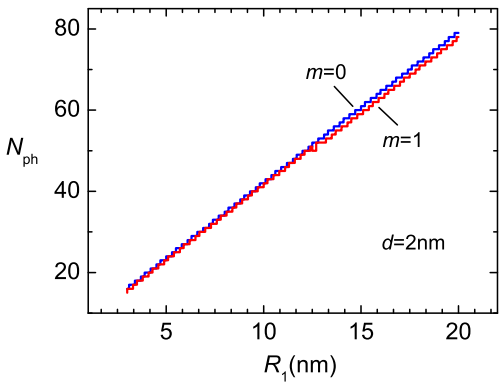

Fig. 12 Number of branches N_{ph} of type 1 phonons with $m = 0$ and $m = 1$ for a core-shell GaAs/$Al_{0.3}Ga_{0.7}$As quantum wire as a function of the core radius. The thickness of the shell is of 2 nm

scattering channels, leading to an increase in scattering rates. Therefore, one can expect the values of mobility to be closer to experimental ones when considering larger size of wires available in experiment.

4 Conclusion

In this paper, the longitudinal optical phonon modes in cylindrical core-shell quantum wires are developed within the dielectric continuum approach. In general, there may exist four types of LO-phonons in a wire in dependence on the concrete parameters of materials the wire is made of and are classified according to the behavior of the radial amplitude of vibrations. Numerical calculations performed for $GaAs/Al_xGa_{1-x}As$ quantum wires with $x = 0.3$ showed that there are only two types, type 1 and type 3, of phonon modes in such wires. These modes have the same oscillating feature of amplitudes in the shell region. The electrostatic potential originating from the optical vibrations has also been obtained. The phonon mode dispersion and the associated potential are modified with the change of the shell thickness and, therefore, influence the electron-phonon interaction. One may expect electron scattering is reduced considerably in the quantum wires having thicker shells due to electron spreading into the shell region since electron scattering rate is governed mainly by the interaction with phonons of type 1 which produce the electrostatic potential emerging significantly in the core. Therefore, higher mobility can be achieved by coating the core with thicker shell.

Acknowledgments The authors would like to thank anonymous reviewers for their valuable comments and suggestions.

References

1. A. Deyasi, S. Bhattacharyya, N.R. Das, Procedia Technol. **4**, 449 (2012)
2. H. Weman, S. Palmgren, K.F. Karlsson, A. Rudra, E. Kapon, D.L. Dheeraj, B.O. Fimland, J.C. Harmand, J. Mater. Sci.: Mater. Electron. **20**, S94 (2009)
3. C. Thelander, P. Agarwal, S. Brongersma, J. Eymery, L.F. Feiner, A. Forchel, M. Scheffler, W. Riess, B.J. Ohlsson, U. Gösele, L. Samuelson, Mater. Today **9**, 28 (2006)
4. S.F. Fischer, G. Apetrii, U. Kunze, D. Schuh, G. Abstreiter, Nat. Phys. **2**, 91 (2006)
5. Y. Huang, X. Duan, Y. Cui, C.M. Lieber, Nano Lett. **2**, 101 (2002)
6. K.J. Vahala, J.A. Lebens, C.S. Tsai, T.F. Kuech, P.C. Sercel, M.E. Hoenk, H. Zarem, Proc. SPIE **1216**, 120 (1990)
7. K.W. Adu, Q. Xiong, H.R. Gutierrez, G. Chen, P.C. Eklund, Appl. Phys. A **85**, 287 (2006)
8. D. Spirkoska, G. Abstreiter, A. Fontcuberta i Moral, Nanotechnology **19**, 435704 (2008)
9. H.J. Xie, C.Y. Chen, B.K. Ma, Phys. Rev. B **61**, 4827 (2000)
10. L. Zhang, Commun. Theor. Phys. **42**, 459 (2004)
11. Z.W. Zuo, H.J. Xie, J. Phys.: Condens. Matter **22**, 025403 (2010)
12. R. Enderlein, Phys. Rev. B **47**, 2162 (1993)
13. C.R. Bennett, B. Tanatar, Phys. Rev. B **55**, 7165 (1997)
14. A.L. Vartanian, Int. J. Mod. Phys. B **20**, 3015 (2006)
15. D.L. Nika, A.I. Cocemasov, D.V. Crismari, A.A. Balandin, Appl. Phys. Lett. **102**, 213109 (2013)
16. J.W. Lee, J. Lee, S. Yi, Y.M. Seo, B.L. Choi, C.h. Yu, C.h.-W. Yang, S. Hwang, S. Kim, D. Whang, E.K. Lee, J. Mater. Chem. A **2**, 12153 (2014)
17. F. Haas, P. Zellekens, M. Lepsa, T. Rieger, D. Grützmacher, H. Lüth, T.h. Schäpers, Nano Lett. **17**, 128 (2017)
18. F. Haas, T. Wenz, P. Zellekens, N. Demarina, T. Rieger, M. Lepsa, D. Grützmacher, H. Lüth, T.h. Schäpers, Sci. Rep. **6**, 24573 (2016)
19. Ö. Gül, N. Demarina, C. Blömers, T. Rieger, H. Lüth, M.I. Lepsa, D. Grützmacher, T.h. Schäpers, Phys. Rev. B **89**, 045417 (2014)
20. G.W. Holloway, Y. Song, C.h.M. Haapamaki, R.R. LaPierre, J. Baugh, Appl. Phys. Lett. **102**, 043115 (2013)
21. D.ario.G. Santiago-Pérez, C. Trallero-Giner, G.E. Marques, Phys. Rev. B **95**, 155317 (2017)
22. N.N. Dat, T.H. Le, Commun. Phys. **24**, 333 (2014)
23. Yu.A. Goldberg, in *Handbook Series on Semiconductor Parameters*, ed. by M. Levinshtein, S. Rumyantsev, M. Shur, Vol. 2 (World Scientific, Singapore, 1999), pp. 1–36
24. M. Abramowitz, I.A. Stegun, Vol. 55, *Handbook of Mathematical Functions, Applied Mathematics Series, 10Th Printing* (National Bureau of Standards, Washington, 1972). Chapter 9
25. P.A. Wolff, G.A. Pearson, Phys. Rev. Lett. **17**, 1015 (1966)
26. C.C. Wang, N.W. Ressler, Phys. Rev. **188**, 1291 (1969)
27. N. Nhu Dat, N. Van Hieu, Phys. Status Solidi **B82**, K39 (1977)
28. W. Götze, P. Wölfle, Phys. Rev. B **6**, 1226 (1972)
29. H.J. Joyce, P. Parkinson, N. Jiang, C.J. Docherty, Q. Gao, H.H. Tan, Ch. Jagadish, L.M. Herz, M.B. Johnston, Nano Lett. **14**, 5989 (2014)